Energy Equip. Sys./ Vol. 10/No. 3/Sep.2022/ 309-326

ENERGY EQUIPSYS

Energy Equipment and Systems

http://energyequipsys.ut.ac.ir
www.energyequipsys.com

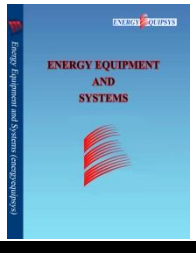

Dynamic simulation of a qanat source heat pump in different climatic conditions

Authors

Maryam Karami[a*]
Hajar Abdshahi[a]

[a] Department of Mechanical Engineering Faculty of Engineering, Kharazmi University, Tehran, Iran

Article history:

Received : 15 September 2021
Accepted : 6 November 2021

ABSTRACT

In this study, the year-round thermal performance of a qanat source heat pump in supplying the required cooling and heating loads of a case study building is investigated. Using TRNSYS software, dynamic simulation of the proposed system is performed in three climate zones including Hot/Dry, Cold/Dry, and Hot/Humid. The heat pump and helical coil heat exchanger inside the qanat water are mathematically modeled in MATLAB, and then, coupled to TRNSYS model to evaluate the system transient performance. It is found that the free energy ratio of the qanat source heat pump Hot/Dry climate zone is on average 21.6% higher than compared to that of the air source heat pump. In cold months, by increasing the temperature of the inlet fluid to the helical coil heat exchanger inside the qanat, the system coefficient of performance increases 15%. The increase of the energy efficiency ratio of the system in the warm months is 7.7%. It is also found the highest coefficient of performance and the lower energy efficiency ratio of the system is obtained in the Hot/Humid climate zone in comparison with the other zones; so that, the energy efficiency ratio of the system in the Cold/Dry and Hot/Dry zones is 48% and 58% higher than that in the Hot/Humid zone, respectively. The annual FER of 63.4%, 63.1%, 56.8%, and 53.3% are obtained in Hot/Dry (Kerman), Cold/Dry (Mashhad), Hot/Dry (Tehran), and Hot/Humid (Bandar Abbas), respectively. These findings suggest that the building energy consumption significantly reduces using the QSHP in all climatic conditions.

Keywords: Qanat Source Heat Pump; Helical Coil Heat Exchanger; Dynamic Simulation; Climatic Conditions; TRNSYS.

1. Introduction

Buildings, as one of the largest primary energy consumers [1], are the main options for potential energy savings and thus, reducing the related environmental problems. In addition to the efficiency enhancement of the building energy systems, using the renewable energy systems to provide the required thermal loads of the buildings received a lot of attention. In this regard, over the past decade, heat pumps as a heat engine, in which heat is transferred from the low temperature source to a higher temperature sink using electrical power, have great appeal for heating and cooling the buildings. A number of different types of environmental heat sources or sinks such as the ambient air, the water sources, the solid ground, or the waste fluids can be used with heat pumps [2].

Water source heat pumps (WSHP) use rivers and streams, lakes and ponds, the sea, or

*corresponding author: Maryam Karami
Department of Mechanical Engineering Faculty of Engineering, Kharazmi University, Tehran, Iran
Email: karami@khu.ac.ir

water wells for rejecting and extracting heat. Several experimental studies have been conducted on the thermal performances of WSHPs. Using the Sihan River, Büyükalaca et al. [3] studied the performance of a heat pump to heat and cool a laboratory space. They reported that the performance of WSHP using Seyhan River is always better than an air source heat pump (ASHP) except at the end of the heating season. Yu et al. [4] reported that the initial investment and operation cost of the SWHP with casted heat exchanger is lower than that of open-loop SWHP. Fei and Pingfang [5] studied the long-term energy performance of a ground water heat pump (GWHP), installed in an apartment building of Wuhan, China. Every two wells had an approximate 80~120m distance and the groundwater level was about 17.8 m~21m. The results indicated that the average system COPs are 2.68 and 3.1 for cooling and heating months, respectively. The thermal performance of a seawater-source heat pump (SWHP) in the Bohai Tianjin Sea in northern China was investigated by Zheng et al. [6] using a new type of floor heating. Using a high-density polyethylene helical coil heat exchanger (HCHE) to exchange heat from the seawater, they found that the average COP of the SWHP is 2.47 at the seawater temperature of 6℃. In another study, they reported that by reducing the water flow rate from 35 to 20 m^3/h, the pumped water temperature increases by about 27% [7]. Athresh et al. [8] used mine water as the heat source/sink of an open-loop WSHP. Their results showed that the COP ranges from 3.5 to 4.5 based on the ambient conditions. Liu et al. [9] used a River-Water Source Heat Pump (RWSHP) System for heating and cooling a large-scale commercial building with an area of 52000 m^2, located by the Huangpu River. The river water has the lowest temperature of 4.5℃ in January and the highest temperature of 32℃ in August. The average system coefficient of performance (COP) was 2.6 and 5.2 in summer and winter, respectively. Besides, the COP of SWHP with Beach Well Infiltration Intake Systems (BWIS) and Helical Coil Heat Exchanger (HCHE) is about 42-27% and 19-35% higher than ASHPs. In another study, Al-Habaibeh et al. [10] found that the average COP increases by increasing the operating cycle time in each run, so that the peak value is 3.72. They also reported that the temperature and depth of coal mine water are the key parameters on the WSHP performance. Wang et al. [11] used a mine-water source heat pump for the residential buildings of a mining community in Henan province, central China. The results showed that the lower condensing temperature in summer and the higher evaporation temperature in winter cause that the mine water- based heat pumps are much more efficient and stable.

Although there are several experimental investigations on WSHPs, relatively few studies have numerically evaluated the thermal performance of these heat pumps. The numerical study of the water-to-water heat pump connected to a groundwater production well, done by Nam and Ooka [12], showed that the system heating and cooling COP reduces respectively by 11.2% and 13.7% by decreasing the groundwater temperature from 18℃ to 12℃. Using numerical simulation software FEFLOW, Liang et al. [13] revealed that the thermal transfer method represents the more consistent results in comparison with two other methods including the energy balance and thermal storage methods because the procedure of groundwater pumping/recharging is considered in the thermal transfer method. Installing and operating guidelines of a GWHP were represented by Kim and Nam [14]. They used individual performance models and system catalog data also considered the effect of groundwater levels, UA values, groundwater flow rates, and temperatures. Their results indicated that the system heating COP increases by increasing the UA values. They also reported that by increasing the groundwater temperature, the system heating COP decreases, whereas the system cooling COP increases. Comparing the performance of lagoon water based heat pump with an ASHP and air cooled chiller indicated that the annual energy saving of about 36.9% and 19.8% is obtained using the proposed system instead of the traditional system and ASHP, respectively [15]. By deployment of Engineering Equation Solver (EES), Amiri et al. [16] concluded that the COP of the underground mine-based SWHP increases from 2.78 to 2.91 by increasing the inlet condenser pressure from

1280 kPa to 1440 kPa. Using a thermodynamic model, Maddah et al. [17] analyzed an industrial wastewater heat pump (WSHP) from the energy, exergy, economic and environmental aspects and found that the CO2 emission reduces by 15.67 and 42.2 tons/year compared to GSHP and ASHP. They also revealed that about 41 GWh/year of heat is recovered from casting factories in Iran, which resulted in the COP of 5.104 and thermal energy production of about 11.8 MW/year.

As the literature review shows, in the studies related to WSHPs, the qanat has received less attention as a energy source or sink. Qanat, which is also called Karis, like a prefabricated structure, can provide easy access to groundwater. It is a low-slope underground canal in which groundwater is transported away from evaporation by gravity [18]. As shown in Fig. 1, main components of the qanat are the mother well, the canal, the access, and output axes [19]. Most of qanats were built in the past; so, there is no need for costly and time-consuming geological studies and excavations to achieve underground water. On the other hand, qanats are usually located near residential areas and their potential can be used for heating and cooling residential spaces.

The first study on the qanat source heat pumps (QSHP) was done experimentally by Delfani et al. [20]. They were designed and installed a test setup in Tehran, Iran, and compared the performance characteristics of the QSHP with an ASHP under the same operating conditions. The results showed that the COP and the energy efficiency ratio (EER) of the QSHP were very stable during the year by variation of 1.5% and 1.8% in cooling and heating modes, respectively, while the COP and EER of the ASHP fluctuated 9% and 6%, respectively, under the same operating conditions.

As above mentioned, although the thermal performance of the WSHPs using various water sources has been assessed, the effect of the qanat as a water source on the WSHP performance has not been yet completely evaluated. Besides, the monthly performance of the WSHPs using different climatic conditions has not been investigated. Therefore, a year-round dynamic simulation of the QSHP is performed using a TRNSYS-MATLAB co-simulator in three different climate zones including Hot/Dry, Cold/Dry, and Hot/Humid zones. The monthly variation of the COP, the energy efficiency ratio (EER), and the free energy ratio (FER) of the QSHP is also investigated and compared with those of the ASHP.

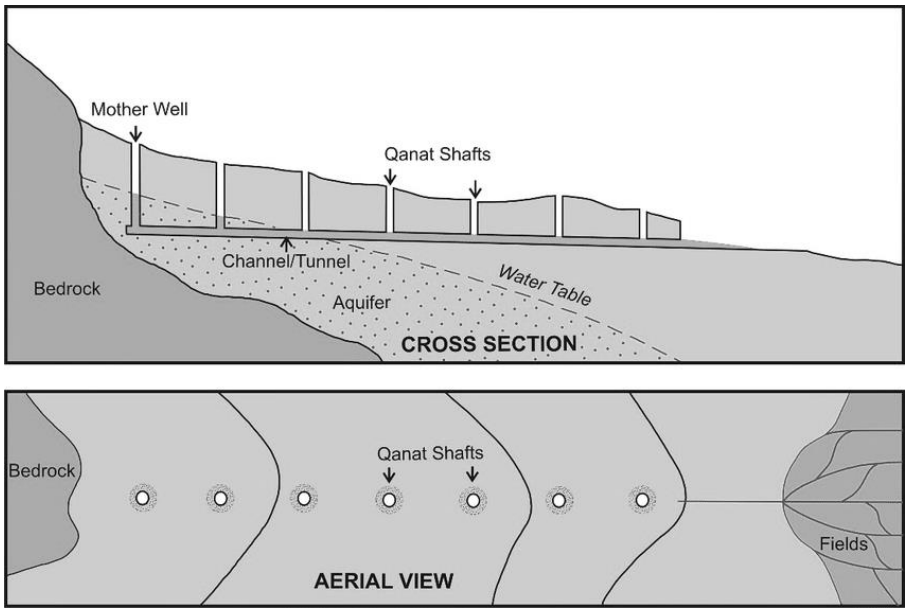

Fig. 1. Qanat components [19]

Nomenclature

A	cross section (m^2)
c_p	Specific heat (J/kg K)
d	Diameter (m)
D	Curvature radius of HCHE (m)
Dn	Dean number
h	Convection heat transfer coefficient (W/m^2K)
h	Enthalpy (kJ/kgK)
He	Helical number
L	Pitch of the helical coils (m)
$\dot{m}$	Flow rate (kg/s)
Nu	Nusselt number
Pr	Prantdl number
$\dot{Q}$	Rate of heat transfer (W)
Re	Reynolds number
T	Temperature (K)
U	Velocity(m/s)
UA	Overall heat transfer coefficient ($kW/℃$)
$\dot{W}$	Rate of work, power (W)

Greek Symbols

ρ	Density (kg/m^3)
μ	Viscosity ($Pa.s$)
x	Length (m)
k	Thermal conductivity ($W/m\ K$)
Δ	Incremental value

Abbreviations

ASHP	Air source heat pump
COP	Coefficient of performance
EER	Energy efficiency ratio
FER	Free energy ratio
GWHP	Ground water heat pump
HCHE	Helical coil heat exchanger
QSHP	Qanat source heat pump
WSHP	Water source heat pump

Subscripts

f	Fluid
i	Node
w	Wall
i	Inner
o	Outer
qw	Qanat water
hp	Refrigerant
WEG	water/Ethylene Glycol
out	Outlet
in	Inlet
evap	Evaporator
com	Compressor
con	Condenser
rm	Room
aux	Auxiliary

2. System description and simulation

Figure 2 shows the schematic of the proposed QSHP system to provide the required cooling and heating demands of the case study building. Table 1 represents the specifications of the case study building. The rate of occupant's activity, the natural ventilation, and the air infiltration into the building are calculated according to ASHRAE 90.1 [21]. As shown in Fig. 2, the HCHE (a) has been inserted into the qanat water. The features of the HCHE, used in this study, are shown in Table 2. The temperature of water/ ethylene glycol solution, as the working fluid of the qanat loop, decreases in the warm months by flowing qanat water around the HCHE, and increases in the cold months. In the heating mode, the heated solution inside the HCHE is conducted to the heat pump by the circulation pump (b) and enters the evaporator (c), in which the refrigerant is evaporated and converted to superheated vapor. The refrigerant vapor enters the compressor (d) and its temperature and pressure increase. By entering the condenser (e), the refrigerant loses its heat to the space and provides the required space heating. By decreasing the refrigerant temperature, it is changed to liquid and enters the expansion valve (g), in which the refrigerant pressure drops and re-enters the evaporator to repeat the cycle.

The thermal performance of the QSHP is dynamically simulated using a TRNSYS-MATLAB co-simulator. In Fig. 3, a flowchart describing the simulation process in this study step by step is shown. The various types of TRNSYS have been used to model the cycle, which is observed in Table 3. The parameters and assumptions considered for each component are also given in Table 3. Since the model of the HCHE and the water-to-air heat pump, which is investigated in this study, do not exist in TRNSYS 16, the models are developed by MATLAB software and then, connected to the TRNSYS model by Type 155. Figure 4 indicates the TRNSYS simulation of the proposed QSHP system.

Table 1. Characteristics of the case study building

Parameter	Value
Thermal resistance of external walls	1.96 m^2K / W
Overall heat transfer coefficient of roof	3.13 m^2K/W
Overall heat transfer coefficient of windows	0.8 m^2K/W
Inside set point temperature in warm months	26℃
Inside set point temperature in cold months	20℃
Area of each apartment unit	100 m^2
Number of apartment units	3
Window-to-Wall Ratio (WWR)	30%
Occupants per each apartment unit	4 persons
Occupant activity level	Seated, light work
Natural ventilation	1 AC/h
Infiltration	0.16 AC/h
Artificial lighting	5 W/m^2

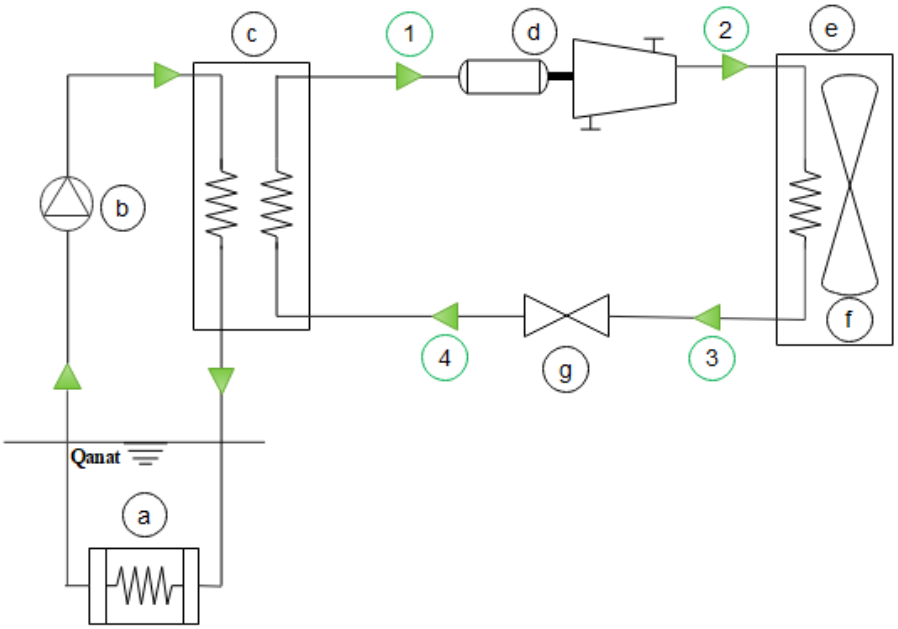

Fig. 2. Schematic of the water-to-air QSHP system (a: HCHE, b: pump, c: evaporator, d: compressor, e: condenser, f: fan, g: expansion valve)

Table 2. Features of HCHE used in this study

Parameter	Value
Material	High density polyethylene
Thermal conductivity	0.49 W/m.K
External diameter of pipes	32 mm
Internal diameter of pipes	29.6 mm
Curvature radius of HCHE	250 mm
Pitch of the HCHE	47 mm
Length of HCHE	1 m

Table 3. List of component features and types used in TRNSYS simulation

Model	Features
Building	• Type 56 estimates the required thermal loads of the building.
Weather information	• Type 109 reads weather data from the weather data file. • Type 69 calculates the effective sky. • Type 33 calculates the dew point temperature, relative humidity, etc. • Annual air temperature variation of the investigated climate zones is shown in Fig. 10.
Circulation pump	• Type 3b • Power coefficient: 0.5 • Maximum power: 1 kw
HCHE+HP	• Type 155 is used to couple the MATLAB model to TRNSYS model.
Plotter and Printer	• Type 65d is a plotter and monitors the simulated data • Type 25a is a printer and exports the simulated data to an external excel file. • Type 24 is an integrator and generates yearly or monthly simulated data.
Equation Model	• The equation model is used to transfer the temperature of the fluid inside the HCHE and the building thermal loads to the MATLAB code in each time step.

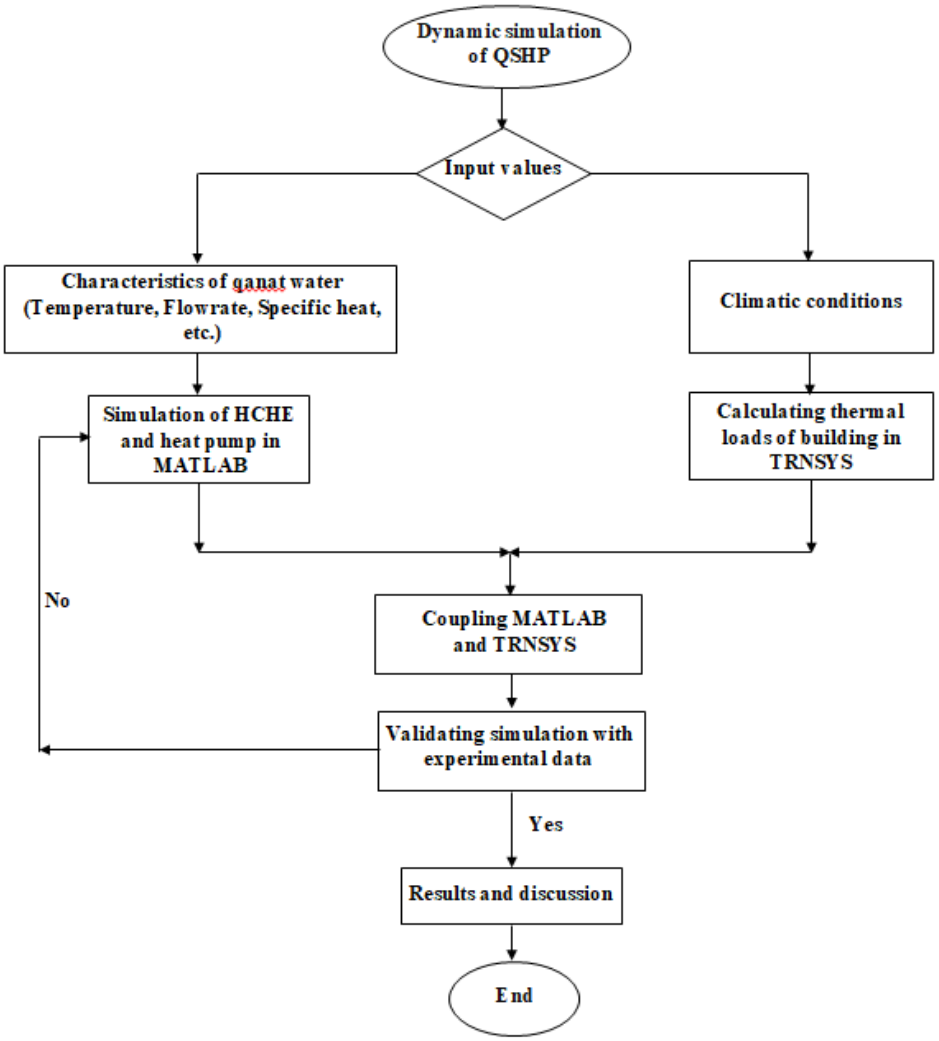

Fig. 3. Flowchart of simulation process

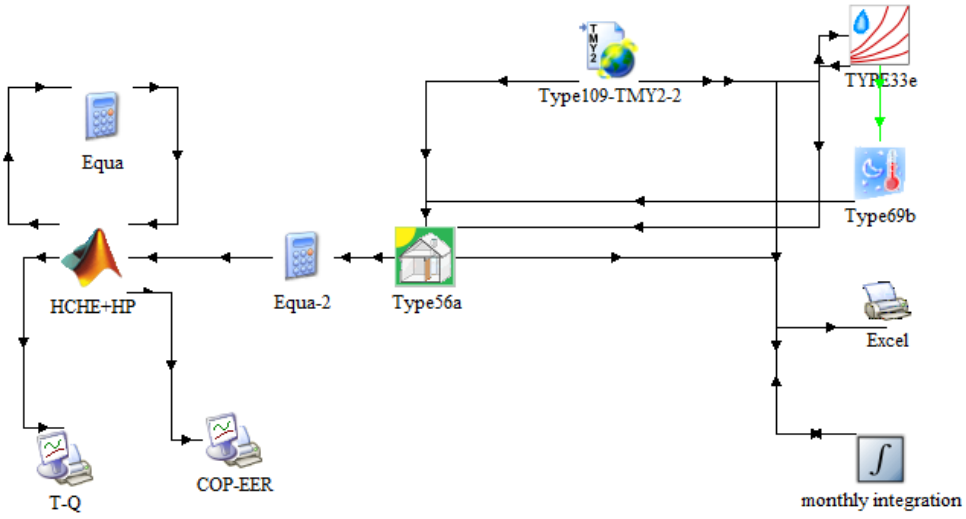

Fig. 4. TRNSYS simulation of the QSHP system

The classical parameter used to describe the heating performance of a heat pump is the coefficient of performance (COP), which is equal to the ratio of condenser heat transfer rate to the compressor power consumption [22]:

$$\mathrm{COP} = \frac{\dot{Q}_{\mathrm{cond}}}{\dot{W}_{\mathrm{comp}}} \tag{1}$$

To evaluate the cooling performance of a heat pump, the energy efficiency ratio (EER) is used. The relation of the EER is the same as the COP, except that, the heat transfer rate is defined in terms of Btu/hr [23].

$$\mathrm{EER} = \frac{\dot{Q}_{\mathrm{evap}}\left(\mathrm{Btu/hr}\right)}{\dot{W}_{\mathrm{comp}}} \tag{2}$$

Another parameter used to evaluate the performance of the heat pump system is the free energy ratio (FER), which is the part of the required load that is provided by the free energy source (ambient, solar energy, geothermal, etc.) and is obtained through the following relations [24]:

$$\mathrm{FER} = \frac{\sum \text{Thermal load} - \sum \text{Input electrical power}}{\sum \text{Thermal load}} \tag{3}$$

$$\sum \text{Input electrical power} = \dot{W}_{\mathrm{comp}} + \dot{W}_{\mathrm{aux}} \tag{4}$$

2.1. HCHE modeling

The heat transfer between the HCHE and qanat water is mathematically modeled using the finite difference method. As indicated in Fig. 5, the HCHE has been divided into "n" sections in the longitudinal direction of the pipe. The following assumptions are considered in modeling:

- Heat transfer is one-dimensional.
- The flow and temperature fields are stable.
- The working fluid is incompressible and has a constant speed.

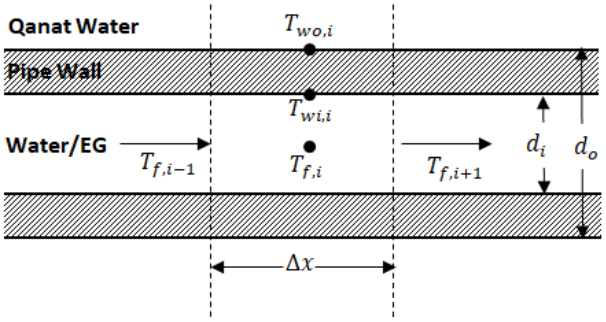

Fig. 5. Schematic of computational domain

The temperature of the water/Ethylene Glycol (WEG) inside the coil, the temperature of the inner and outer walls of the coil was indicated by T_f, T_{wi} and T_{wo}. For the outer wall of the pipe, the energy balance equation is as follows [25]:

$$k_w A_o \frac{\left(T_{wo,i-1} - T_{wo,i}\right)}{\Delta x} + 2\pi k_w \Delta x \frac{\left(T_{wi,i} - T_{wo,i}\right)}{\ln \frac{d_{out}}{d_{in}}} - h_{qw} \pi d_o \Delta x \left(T_{wo,i} - T_{qw}\right) - k_w A_o \frac{\left(T_{wo,i} - T_{wo,i+1}\right)}{\Delta x} = 0 \quad (5)$$

where A_o is the cross section of circular ring of "i" node grid [26]:

$$A_o = \pi \left(\frac{d_o + d_i}{2}\right) \Delta x \quad (6)$$

In Eq. (1), T_{qw} is the qanat water temperature and h_{qw} is the convective heat transfer coefficient of the qanat water and determined by using the following equations [27]:

$$h_{qw} = \frac{Nu_{qw} k_{qw}}{d_o} \quad (7)$$

$$Nu_{qw} = 0.66\ Re^{0.529} \quad (8)$$

For the inner wall of the pipe, the energy balance equation is as following:

$$k_w A_i \frac{\left(T_{wi,i-1} - T_{wi,i}\right)}{\Delta x} + h_{f,i} \pi d_i \Delta x \left(T_{wi,i} - T_{f,i}\right) - 2\pi k_w \Delta x \frac{\left(T_{wi,i} - T_{wo,i}\right)}{\ln \frac{d_o}{d_i}} - k_w A_i \frac{\left(T_{wi,i} - T_{wi,i+1}\right)}{\Delta x} = 0 \quad (9)$$

where k_w is the thermal conductivity of HCHE pipe and A_i is the cross section of circular ring of "i" node grid:

$$A_i = \frac{\pi}{16}\left[4d_o^2 - \left(d_o + d_i\right)^2\right] \quad (10)$$

The energy balance equation for the working fluid is as following:

$$\frac{\pi}{4} d_i^2 U \rho_{f,i} c_{f,i} \frac{\left(T_{f,i-1} - T_{f,i+1}\right)}{2} - h_{f,i} \pi d_i \Delta x \left(T_{f,i} - T_{wi,i}\right) = 0 \quad (11)$$

where $h_{f,i}$ is the convection heat transfer coefficient is determined is as follows [27]:

$$h_{f,i} = \frac{Nu_i k_f}{d_i} \quad (12)$$

For the laminar region($Re \leq 2300$), the Nusselt number of helical coil is calculated as following [28]:

$$Nu_i = \left[\left(\left(\frac{48}{11} + \frac{51/11}{\left(1 + 1342 / Pr_{f,i} * He_{f,i}^2\right)^2} + 1.816 * \left(\frac{He_{f,i}}{1 + 1.15 / Pr_{f,i}}\right)^{3/2}\right)\right)\right]^{1/3} \quad (13)$$

$$Pr_{f,i} = \frac{\lambda_{f,i}}{C_{pf,i} * \rho_{f,i}} \quad (14)$$

$$He_{f,i} = \frac{De_{f,i}}{\left(1 + \left(L / 2\pi D\right)^2\right)^{0.5}} \quad (15)$$

$$De = Re_{f,i} \left(d / D\right)^{0.5} \quad (16)$$

where Pr, He and Dn are the Prantdl number, Helical number and Dean number, respectively. The boundary conditions of Eq. (6) are as following:

$$i = 0,\ T_{f,0} = T_{inlet}$$
$$i = n,\ \partial T / \partial x = 0 \quad (17)$$

To estimate the temperature distribution of the working fluid along the HCHE, Eqs. (5), (9), and (11) are solved using the boundary conditions (Eq. (17)) and the iteration method.

2.2. Heat pump modeling

The compression water/EG-to-air heat pump connected to the qanat is modeled in MATLAB using thermodynamic analysis. The compressor power consumption is determined using the following relation [22]:

$$\dot{W}_{comp} = \frac{\dot{m}_{hp}\left(h_2 - h_1\right)}{\eta_{comp}} \quad (18)$$

The compressor efficiency is assumed to be 80%. The heat transfer rate in the condenser and evaporator is obtained using the following relations:

$$\dot{Q}_{cond} = \dot{m}_{hp}\left(h_2 - h_3\right) \quad (19)$$

$$\dot{Q}_{evap} = \dot{m}_{hp}\left(h_1 - h_4\right) \quad (20)$$

Based on the heat transfer mode, i.e. heating or cooling, the heat transfer rate in the

condenser and evaporator is equal with the heat loss or gain of water/EG solution in HCHE:

$$\dot{Q}_{eva,cond} = \dot{m}_{WEG} C_{WEG} \left(T_{WEG,out} - T_{WEG,in} \right) \quad (21)$$

where $\dot{m}_{WEG}$ and C_{WEG} are the mass flow rate of water/EG solution and its specific heat, respectively.

The effectiveness of the condenser or the evaporator as the heat exchanger is calculated using $\varepsilon - NTU$ method [27]:

$$\varepsilon = \frac{q_{(cond,eva)}}{q_{max(cond,eva)}} = 1 - \exp\left(-\frac{UA}{C_{p,min}} \right) \quad (22)$$

where the maximum heat transfer through the heat exchanger is calculated as follows:

$$q_{max,eva} = C_{p,min} \left(T_{HCHE,in} - T_4 \right) \quad (23)$$

$$q_{max,cond} = C_{p,min} \left(\frac{T_2 + T_3}{2} - T_{rm} \right) \quad (24)$$

where $T_{HCHE,in}$ is the fluid inlet temperature to the HCHE and T_{rm} is the room air temperature. The high side temperature of the condenser is considered the average temperature of the refrigerant throughout the condenser [29]. The heat transfer in the evaporator and condenser was then calculated by combining equations (18-20) and (22-23).

The expansion valve is modeled as a constant enthalpy process:

$$h_3 = h_4 \quad (25)$$

The valve is moderated so that the flow through the compressor has a 5°C superheat temperature. In this study, the overall heat transfer coefficients, UA, for both heat exchangers were assumed to be 0.2 kW/°C [29].

2.3. Model Validation

To evaluate the accuracy of modeling results, a comparison between numerical and experimental results has been performed. Delfani et al. [20] studied the COP and functional characteristics of the heating and cooling system connected to the qanat [20]. Figure 6 shows a comparison between the experimental and numerical COP of the QSHP. As can be seen, the results have a maximum error of 10%, which confirms the accuracy of the simulation.

3. Results and discussion

In this section, after comparing the monthly COP, EER, and FER of the QSHP and ASHP in Hot/Dry climate zone (Tehran), the effect of HCHE inlet fluid temperature and climatic conditions on the QSHP performance is evaluated.

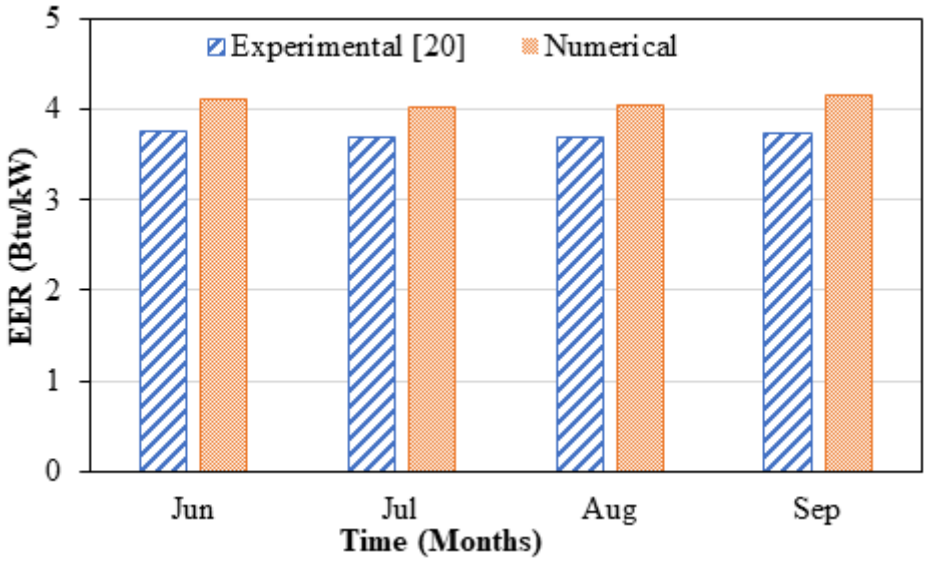

Fig. 6. Experimental [20] and numerical values of system COP

3.1. Comparison of QSHP and ASHP performance

Before presenting the results, it should be noted that all figures are presented for the HCHE fluid flow rate of 2 l/min. In Fig. 7, the variation of the COP and EER of the QSHP and the ASHP is indicated. As shown, the EER and COP of the QSHP are more stable than the ASHP, because the qanat water temperature is more uniform than the ambient temperature, as was reported in Ref. [20]. The maximum and minimum COP of the QSHP are 2.23 in April and 1.98 in January, respectively; while, these values for the ASHP are 2.11 and 1.31 at the same months with the QSHP. As can be seen in Fig. 7 (b), the EER of the QSHP decreases from 6.92 Btu/kW in September to 6.3 Btu/kW in July; while, the EER of the ASHP reduces from 5.41 Btu/kW in September to 4.43 Btu/kW in August. It should be noted that the heating load in October and the cooling load in May are very low and therefore, there is no need to use the QSHP. It can be seen that the performance of QSHP is better than ASHP, because the heat capacity of qanat water is much more than air.

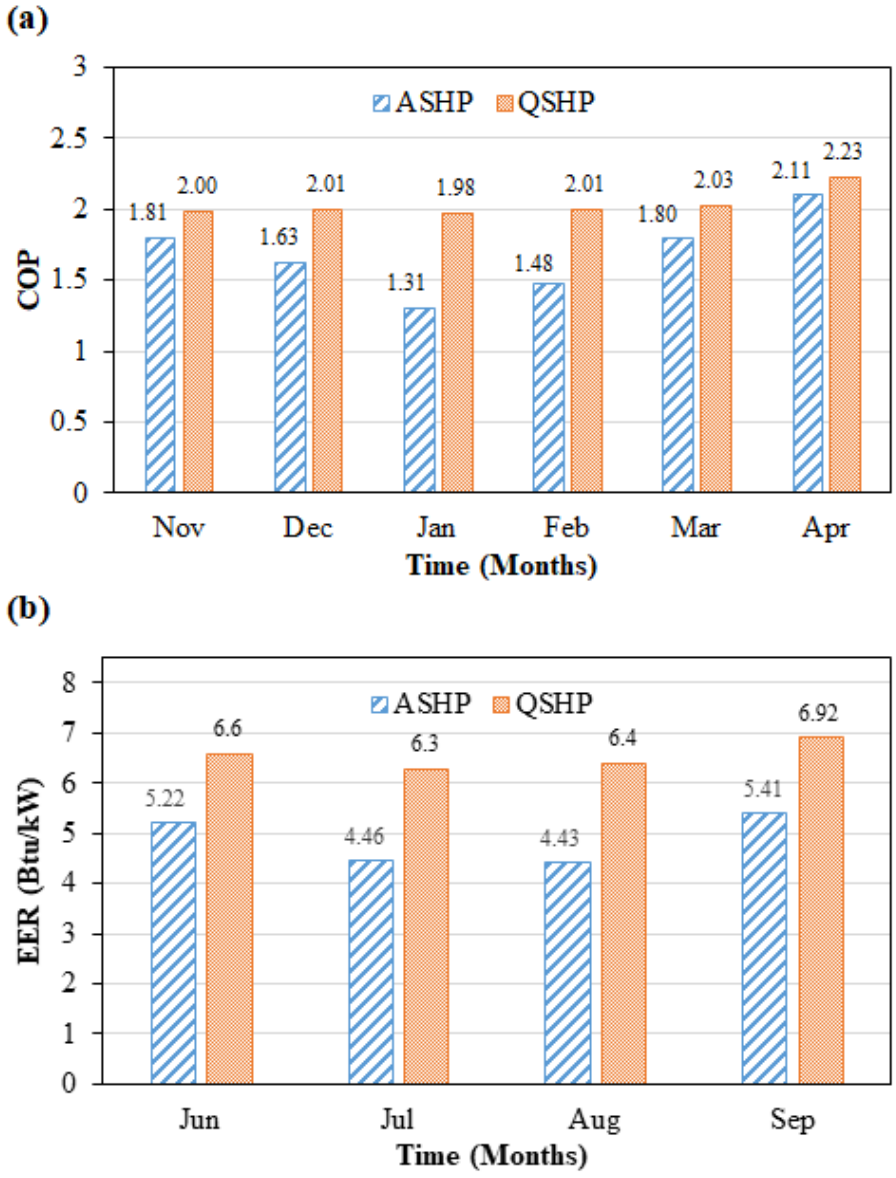

Fig. 7. Monthly variation of (a) COP and (b) EER

Figure 8 displays the monthly variation of the FER of the QSHP and the ASHP. It is found that the maximum and the minimum free energy ratios of the QSHP in Hot/Dry climate zone are 40% and 52% higher than those of the ASHP, respectively. This means that the heating (or cooling) capacity of the QSHP is higher than that of the ASHP because the compressor power of both systems was considered equal. The maximum and minimum FER of the QSHP are 86.3% in April and 59.9% in January, respectively. These values are 31.6% and 25% higher compared to those of the ASHP at the same months. It is interesting to note that the higher difference between the FER of ASHP and QSHP is occurred in cold months in comparison with warm months because of the low ambient temperature, which has negative effect on the heat pump performance.

3.2. Effect of HCHE inlet fluid temperature

In Fig. 9, the effect of the HCHE inlet fluid temperature on the COP and the EER of the QSHP is shown. Figure 9 (a) indicates that the system COP increases by increasing the inlet fluid temperature, due to the increase of the heat transfer in the evaporator and thus, the reduction of compressor power consumption; so that, by variation of inlet fluid temperature from 12℃ to 18℃, the COP enhances by 14.9%, 5.2%, 4.1%, 5.7%, 15.1%, and 8.1% in November, December, January, February, March, and April, respectively. Also, it is interesting to note that the variation of the HCHE inlet fluid temperature has a greater effect on the COP at the lower heating load; so that, the maximum enhancement is obtained in April. This is because most of the condenser heat transfer rate is supplied by the evaporator, and thus, the compressor power consumption reduces. Also, in January, the required heating load is more than other months, and compared with the other months, the compressor power consumption increases; so the COP is less than the other months. In the warm months, the system EER increases by 1%, 2%, 7.7%, and 0.9% in June, July, August, and September by increasing the inlet fluid temperature from 22℃ to 28℃.

Figure 10 shows the FER for different HCHE inlet temperatures in cold and warm months. Figure 10 (a) indicates that the FER increases by increasing the HCHE inlet fluid temperature. The highest FER, i.e. 61.9%, occurs in April at the HCHE inlet fluid temperature of 18℃, because the heating load and therefore, the evaporator heat transfer rate is the lowest compared to the other months. The lowest FER, i.e. 51.8%, occurs in January at the HCHE inlet fluid temperature of 12℃, because of the highest heating load and thus, the highest compressor power consumption than the other months. The FER enhancement in November, December, January, February, March, and April by the variation of the inlet fluid temperature from 12℃ to 18℃, are 5.8%, and 4.5%, 3.6%, 4.8%, 4.2%, and 5.7%, respectively. The results of Fig. 10 (b) reveal that the highest and the lowest FER belong to June and August, respectively. In warm months, the FER is higher at the lower HCHE inlet fluid temperature, because the condenser heat transfer rate is higher; therefore, the compressor consumes the lower power. As it can be seen the FER has the same trend as the COP and EER.

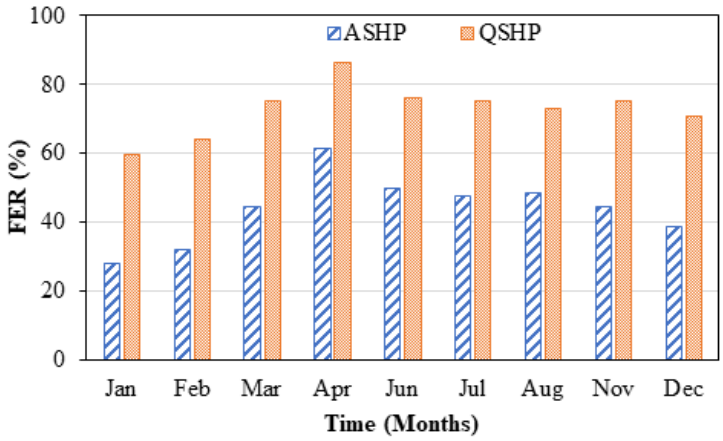

Fig. 8. Monthly variation of the system FER

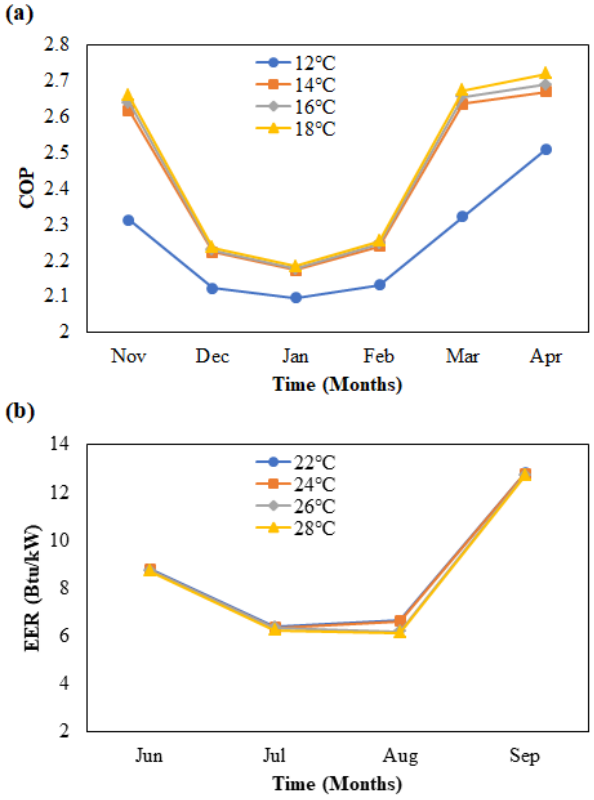

Fig. 9. Effect of inlet fluid temperature to HCHE on (a) COP and (b) EER of QSHP

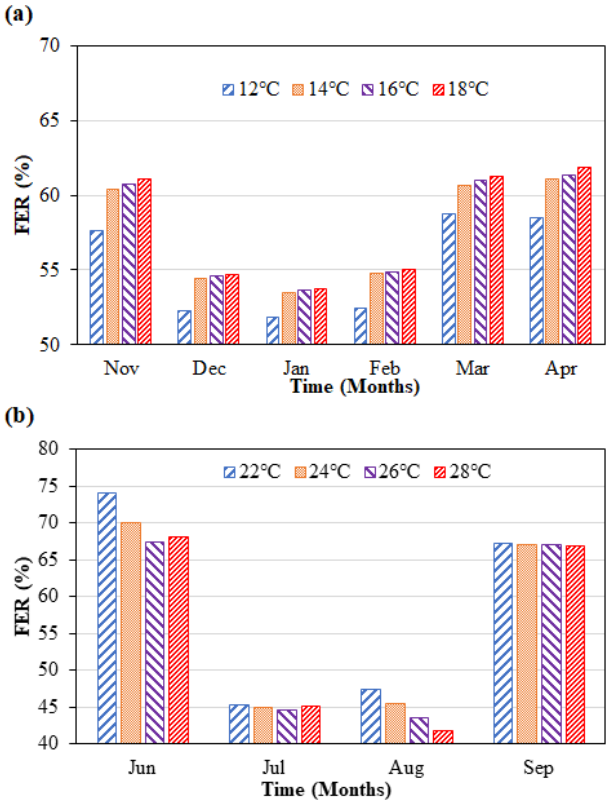

Fig. 10. Effect of the HCHE inlet fluid temperature on the FER of QSHP in (a) cold and (b) warm months

3.3.Effect of climatic conditions

To study the effect of climatic conditions on the COP, EER, and FER of the QSHP, the thermal performance of the system has been numerically studied in three different climatic zones including Hot/Dry zone (Kerman and Tehran), Cold/Dry zone (Mashhad), Hot/Humid zone (Bandar Abbas). The characteristics of the climate zones are listed in Table 4.

Figure 11 (a) shows the monthly average of the mean ambient temperature in the investigated climate zones. As shown, the ambient temperatures in the Hot/Hamid zone (Bandar Abbas) are higher than that in other zones, of which the minimum and maximum are 18℃ in January and 36℃ in July. These values for Cold/Dry zone (Mashhad), Hot/Dry zone (Kerman), and Hot/Dry zone (Tehran) are 0℃ and 27.7℃, 4.5℃ and 28.9℃, 6℃ and 33.5℃, respectively.

The thermal loads of the building have shown in Fig. 11 (b). It is found that the cooling load of the building in the Hot/Hamid zone (Bandar Abbas) is higher than that in the other zones. The maximum cooling load of the building in the Hot/Hamid zone (Bandar Abbas) is 2.5 kW in August, while this value in the Cold/Dry zone (Mashhad), Hot/Dry zone (Kerman), and Hot/Dry zone (Tehran) are 0.54 kW, 0.8 kW, and 2.16 kW, respectively. As expected, the heating load of the building in Cold/Dry zone (Mashhad) is higher than that in other climate zones. The maximum heating load in the Hot/Hamid zone (Bandar Abbas), the Cold/Dry zone (Mashhad), the Hot/Dry zone (Kerman), and the Hot/Dry zone (Tehran) are 0.5 kW, 8.15 kW, 4.7 kW, and 6.25 kW, respectively. It should be noted that the building in the Hot/Hamid zone (Bandar Abbas) requires space heating only in January and February.

Figures 12 represent the system COP, the heat transfer rates, and the power consumption in different climate zones in cold months. As expected, the condenser heat transfer rate in the Hot/Dry zone (Kerman) is lower than that in the Cold/Dry zone (Mashhad), because of the lower heating load (see Fig. 11 (b)). The maximum difference of 42.5% occurs in January. In both climate zones, the highest COP of 4.69 and 5.23 is obtained in April, in which the condenser heat transfer rate is the lowest and thus, the compressor has the minimum power consumption. Looking at Figs. 12 (a), (b), and (c), it is found that higher heating load results in higher compressor power consumption, and thus, the system COP in January is the lowest, which is about 6% higher in Hot/Dry zone (Kerman) in comparison with that in Cold/Dry zone (Mashhad). It should be noted that in the Hot/Humid zone (Bandar Abbas), the heating loads are very low and required only in two months of January and February, in which the system has the larger COP in comparison with other zones, i.e. 5.23 in January and 5.98 in February.

Figure 13 shows the impact of climatic conditions on the system EER, the heat transfer rates, and the power consumption in warm months. As observed, the highest EER for Cold/Dry zone (Mashhad) and Hot/Dry zone (Kerman) occurs in September (about 13.3); however, the highest EER in the Hot/Humid zone (Bandar Abbas) is obtained in October, because of the lower cooling load and thus, the lower heat transfer rate of the evaporator. It is also found from Fig. 13 (d) that in the Hot/Humid zone, the cooling load is required from May to October, while in the Cold/Dry zone (Mashhad) and Hot/Dry zone (Kerman), it is required from June to September. The highest and lowest system EERs are 13.58 and 6.13, which occur in October and August, respectively, in the Hot/Humid zone (Bandar Abbas). It should be noted that the maximum cooling load in the Hot/Humid zone occurs in August (see Fig. 11 (b)).

In Fig. 14, the system FERs in the Hot/Dry zone (Tehran and Kerman), Hot/Humid zone (Bandar Abbas), and Cold/Dry zone (Mashhad) are compared. As observed, in the warm months (June, July, and August), the FER is smaller in Hot/Humid zone (Bandar Abbas) than that in the other climate zones, due to the higher cooling load, which leads to the larger compressor power consumption, whereas the FER in the Hot/Humid zone (Bandar Abbas) is higher compared to the other zones in January and February, due to less heating load. In June, for instance, the system free energy ratio in the Hot/Humid zone is 27% and 28.5% less than that in the Hot/Dry and Cold- Dry zones,

respectively. In the rest of the cold months, the FER of the system in the Cold/Dry zone (Mashhad) is higher than that in the Hot/Dry zone (Kerman) because of more heating load.

The maximum and minimum FER are about 75.3% and 43.3%, which are obtained respectively in Cold/Dry and Hot/Humid zones in April and August. The annual FER of 63.4%, 63.1%, 56.8%, and 53.3% are obtained in Hot/Dry (Kerman), Cold/Dry (Mashhad), Hot/Dry (Tehran), and Hot/Humid (Bandar Abbas), respectively. This indicates that considerable energy savings are achieved using the QSHP for supplying the energy damnd of the buildings in all climatic conditions.

Table 4. Geographical characteristics of the climate zone [30]

Climate zone	City	Sea level (m)	Longitude (°E)	Latitude (°N)
Hot/Dry	Tehran	1191	35.68	51.32
Hot/Dry	Kerman	1754	56.97	30.25
Cold/Dry	Mashhad	999	59.63	36.27
Hot/Humid	Bandar Abbas	10	56.37	27.22

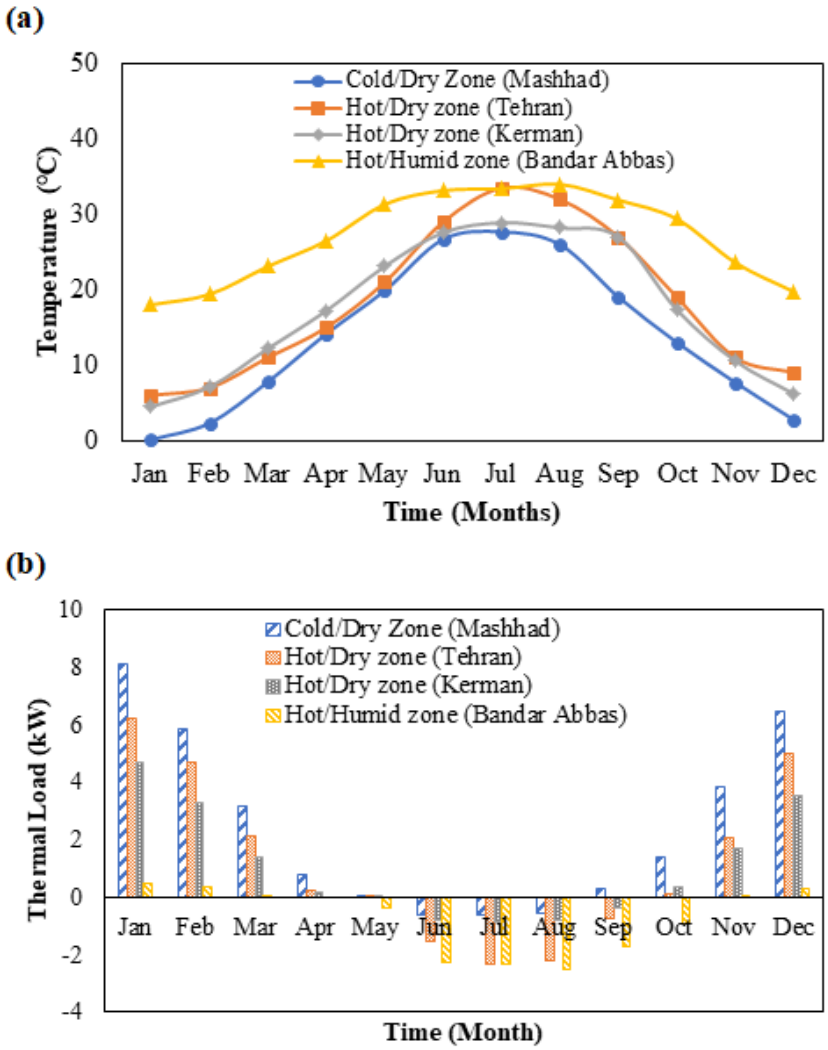

Fig. 11. Monthly variation of (a) mean ambient temperature and (b) heating and cooling loads of the case study building in different climate zones

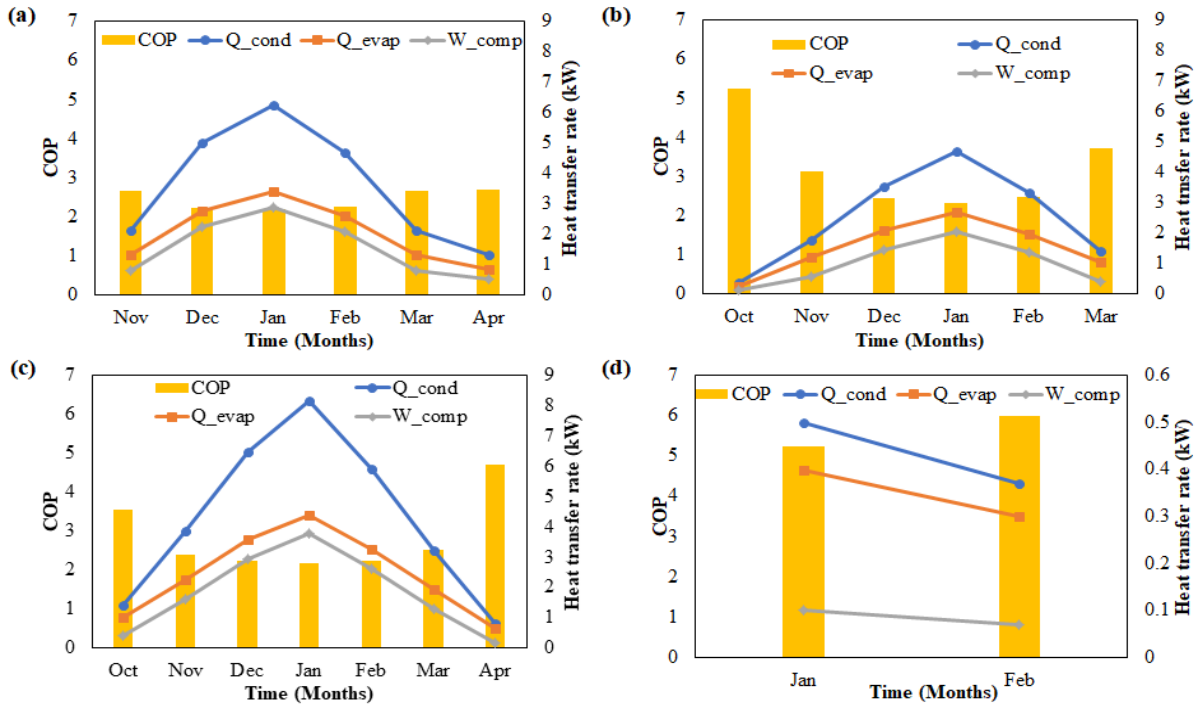

Fig. 12. Monthly variation of system COP and heat transfer rate in (a) Hot/Dry zone (Tehran), (b) Hot/Dry zone (Kerman) (c) Cold/Dry zone (Mashhad), (d) Hot/Humid zone (Bandar Abbas)

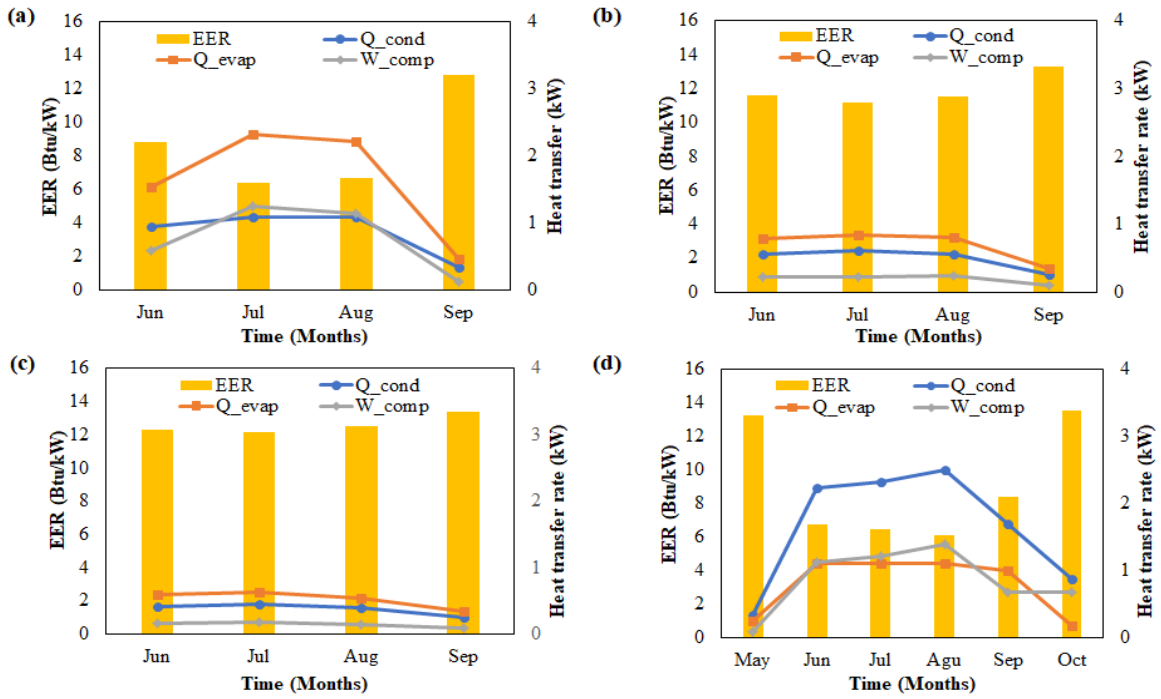

Fig. 13. Monthly variation of system EER and heat transfer rate in (a) Hot/Dry zone (Tehran), (b) Hot/Dry zone (Kerman), (c) Cold/Dry zone (Mashhad), and (d) Hot/Humid zone (Bandar Abbas)

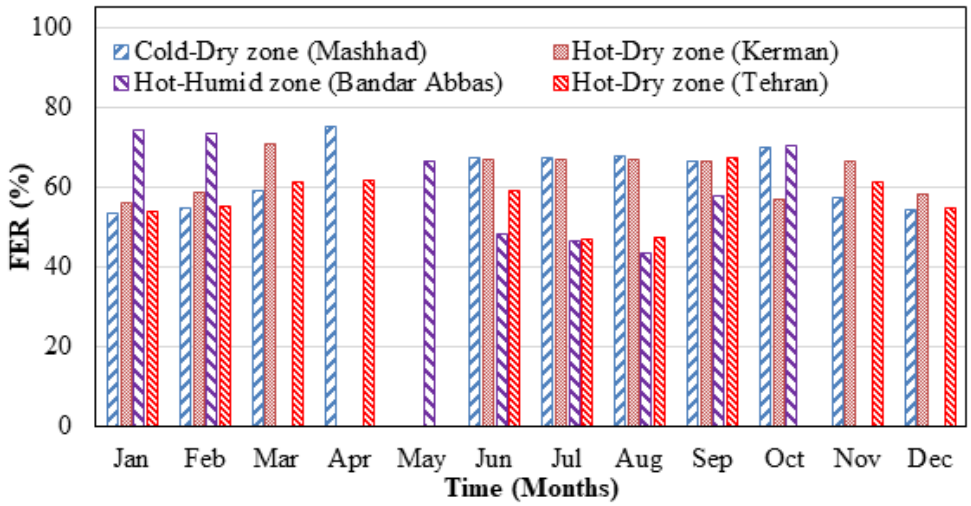

Fig. 14. System FER in different climate zones

4. Conclusions

In this paper, the year-round thermal performance of the QSHP is investigated and compared with that of the ASHP in different climate zones using the TRNSYS-MATLAB co-simulator. The results are summarized as follows:

- The thermal performance of the QSHP is noticeably improved in comparison with the ASHP; so that, in cold months, the highest and lowest COP of the QSHP is 5% and 34% higher than that of the ASHP, respectively. In warm months, the highest and the lowest EER of the QSHP system are 20% and 29% more than that of the ASHP, respectively. Furthermore, the maximum and the minimum FERs of the QSHP system are 31.6% and 25% higher than those of the ASHP system, respectively.
- The HCHE inlet fluid temperature has a significant effect on the QSHP performance because of the variation of the heat transfer rate in the heat exchangers of the system. By increasing the temperature of the inlet fluid to the HCHE inside the qanat from 12℃ to 18℃ in the cold months, the system monthly COP increases between 4.1% - 15.1%. By reducing the HCHE inlet fluid temperature from 28℃ to 22℃ in the warm months, the system EER enhancement is between 0.9% - 7.7%.
- The system COP of about 2.19, 2.31, 2.17, and 5.23 in respectively Hot/Dry zone (Tehran), Hot/Dry zone (Kerman), Cold/Dry zone (Mashhad), and Hot/Humid zone (Bandar Abbas) confirmed that the lower the heating load required, the better the heat pump performance the higher COP. The same trend is shown about system EER, which is higher at the lower the cooling load.
- Because of the lower thermal load, the system FER in the Hot/Humid zone (Bandar Abbas) is lower than that in other climate zones in warm months; whereas in the cold months, the Hot/Humid zone (Bandar Abbas) has a higher FER than the other climate zones. For example, the FER of the Hot/Humid zone (Bandar Abbas) is 9% and 10.9% less than the FERs of the Cold/Dry zone (Mashhad) and Hot/Dry zones (Kerman) in cooling conditions, respectively. Also, in heating condition its FER is 8.6% and 8.2% more than the FERs of the Cold/Dry (Mashhad) and Hot/Dry zones (Kerman).
- Based on the obtained FER, the energy consumption of the case study building reduces by 47.4%-67.2% using the QSHP as the heating and cooling system in Hot/Dry zone (Tehran). The energy savings in Hot/Dry zone (Kerman), Cold/Dry zone (Mashhad), and Hot/Humid zone (Bandar Abbas) varies

between 56%-71%, 53.5%-75%, 45.3%-74.2%, respectively.

- The results show that using the QSHP for providing the thermal loads of the buildings can significantly reduce the building energy consumption and the related environmental problems in different climatic conditions.

References

[1] DeForest N, Shehabi A, Selkowitz S, Milliron DJ (2017) A comparative energy analysis of three electrochromic glazing technologies in commercial and residential buildings. Applied Energy 192: 95-109.

[2] Spitler JD, Mitchell MS (2016) Surface water heat pump systems, Editor(s): Simon J. Rees, Advances in Ground-Source Heat Pump Systems. Woodhead Publishing: 225-246.

[3] Büyükalaca TYO, Ekinci F (2003) Experimental investigation of Seyhan River and dam lake as heat source–sink for a heat pump. Energy 28: 157–169.

[4] Yu J, Zhang H, You S, Dong L (2012) Heat Transfer and Economic Analysis of Seawater-Source Heat Pump System with Casted Heat Exchanger. Asia-Pacific Power and Energy Engineering Conference, Shanghai, China: 1-5.

[5] Fei L, Pingfang H (2012) Energy and Exergy Analysis of a Ground Water Heat Pump System. Physics Procedia 24: 169 – 175.

[6] Zheng W, Zhang H, You S, Yu T (2016) Heat transfer performance of a seawater-source heat pump with radiant floor heating system incold areas of China. Science and Technology for the Built Environment 23 (3): 469-477.

[7] Zheng W, Ye T, You S (2015) The thermal performance of seawater-source heat pump systems in areas of severe cold during winter. Energy Convers. Manag. 90: 166-174.

[8] Athresh AP, Al-Habaibeh A, Parker K (2016) The design and evaluation of an open loop ground source heat pump operating in an ochre-rich coal mine water environment. International Journal of Coal Geology 164: 69–76.

[9] Liu Z, Tan H, Lia Z (2017) Heating and Cooling Performances of River-Water Source Heat Pump System for Energy Station in Shanghai. Procedia Engineering 205: 4074–4081.

[10] Al-Habaibeh A, Athresh AP, Parker K (2018) Performance analysis of using mine water from an abandoned coal mine for heating of buildings using an open loop based single shaft GSHP system. Applied Energy 211: 393–402.

[11] Wang H, Duan H, Chen A (2018) Energy saving analysis on mine-water source heat pump in a residential district of Henan province, central China. IOP Conf. Series: Earth and Environmental Science 121: 052093.

[12] Nam Y, Ooka R (2010) Numerical simulation of ground heat and water transfer for groundwater heat pump system based on real-scale experiment. Energy and Buildings. 42: 69-75.

[13] Liang J, Yang Q, Liu L, Li X (2011) Modeling and performance evaluation of shallow ground water heat pumps in Beijing plain, China, Energy and Buildings 43: 3131–3138.

[14] Kim J, Nam Y (2016) A Numerical Study on System Performance of Groundwater Heat Pumps. Energies 9 (1):4.

[15] Schibuol L, Scarpa M (2016) Experimental analysis of the performances of a surface water source heat pump. Energy and Buildings 113: 182-188.

[16] Amiri L, Madadian E, Hassani FP (2019) Energo- and exergotechnical assessment of ground-source heat pump systems for geothermal energy production from underground mines. Environmental Technology 40 (27): 3534–3546.

[17] Maddah S, Deymi-Dashtebayaz M, Maddah O (2020) 4E analysis of thermal recovery potential of industrial wastewater in heat pumps: An invisible energy resource from the iranian casting industry sector. Journal of Cleaner Production 265: 121824.

[18] Mostafaeipour A (2010) Historical background, productivity and technical issues of qanats. Water Hist. 2: 61–80.

[19] Soroush M, Mehrtash A, Khazraee E, Ur JA (2020) Deep Learning in Archaeological Remote Sensing: Automated Qanat

Detection in the Kurdistan Region of Iraq. Remote Sens.12: 500.

[20] Delfani S, Esmaeelian J, Karami M (2021) Experimental investigation on the thermal performance of a qanat-source heat pump. Geothermics 80: 101933.

[21] Standard, ASHRAE (2013). Standard 90.1-2013. Energy Standard for Buildings Except Low-Rise Residential Buildings.

[22] Cengel Y, Boles M (2014) Thermodynamics: An Engineering Approach, McGraw-Hill Education, 8th Edition.

[23] Valizade L (2014) Ground Source Heat Pumps. Clean Energy Technol. 1: 136.

[24] Chu J, Choi W, Cruickshank CA, Harrison SJ (2014) Modeling of an Indirect Solar Assisted Heat Pump System for a High Performance Residential House. Sol. Energy Eng. 136 (4): ES2013-18222, V001T01A011.

[25] Wu Z, You S, Zhang H, Fan M (2019) Mathematical Modeling and Performance Analysis of Seawater Heat Exchanger in Closed-Loop Seawater-Source Heat Pump System. Energy Eng 145 (4).

[26] Zheng W, Zhang H, You S, Ye T (2016) Numerical and experimental investigation of a helical coil heat exchanger for seawater-source heat pump in cold region. Heat Mass Transf. 96: 1–10.

[27] Bergman ASL, Lavine AS, Incropera FP, DeWitt DP (2011) Fundamentals of heat and mass transfer. Wiley, 8th edition.

[28] Kakac S, Liu H, Pramuanjaroenkij A (2012) Heat Exchangers: Selection, Rating, and Thermal Design. 3rd edition, CRC Press.

[29] Bridgeman A, (2010) Experimental Analysis of an Indirect Solar Assisted Heat Pump for Domestic Water Heating. Thesis (Master, Mechanical and Materials Engineering), Queen's University.

[30] Standard, ASHRAE (2009). Fundamentals. Research Project RP-1453: Updating the ASHRAE climatic data for design and standards.